Influence of Geometry on the Number of Buckles in Cylinders

RICHARD L. DE NEUFVILLE*
Massachusetts Institute of Technology, Cambridge, Mass.

Variation of n

THE variation of n with R/t and L/R, obtained from published experimental data,[1, 2] is shown in Fig. 1. It can be seen that the plot is divisible into two zones. Below a critical value of R/t, the observed buckling stress, which is the total axial load divided by the cross-sectional area, equals or approaches the yield stress and thus defines the plastic region. The elastic region is defined by all values of R/t greater than the critical.

In the plastic region, n increases directly as R/t. No effect of length could be observed in this region.

In the elastic region, n continues to increase as R/t, but this increase is at a much slower rate. It is also possible to observe that n decreases as L/R increases.

Analysis: Plastic Region

Plastic buckling is precipitated by the yielding of the material rather than by the relation of the load and the geometry. Replacing the buckling stress by the yield stress in σ/σ_{cl}, the ratio of the actual buckling stress to the theoretical buckling stress, we see that, as shown in Fig. 2, σ/σ_{cl} is directly proportional to R/t:

$$\sigma/\sigma_{cl} = \sigma_y/(0.6\ E\ t/R) = (\sigma_y/0.6\ E)\ (R/t)$$

With regard to the variation of n, it is appropriate to recall that the postbuckling load deflection curve proposed by von Karman and Tsien[3] is an envelope to the curves representing the nonlinear behavior of configurations with different n, the lower n values corresponding to lower σ/σ_{cl} values. This behavior is shown in Fig. 3 and has been confirmed experimentally by Thielemann.[4] It is therefore reasonable that n decrease as σ/σ_{cl} decreases, which is the result obtained in the plastic zone.

The critical R/t that divides plastic and elastic behavior may be found. Considering steel as an example, point A in Fig. 2 is located at:

$$R/t = 0.6\ (E/\sigma_y) = 0.6\ (3 \times 10^7/3 \times 10^4) = 600$$

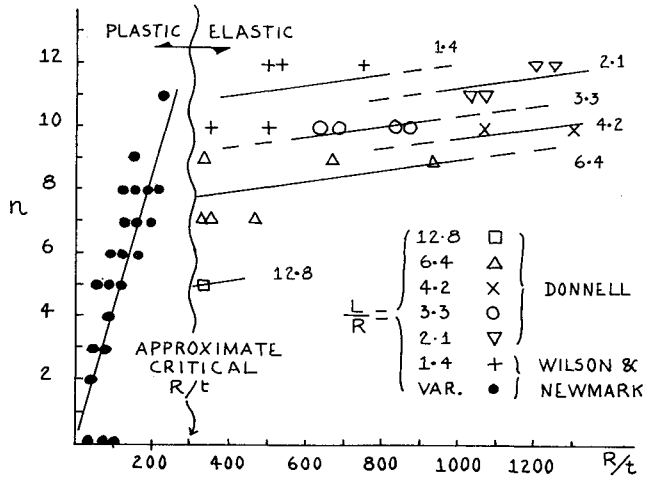

Fig. 1 Variation of n with R/t.

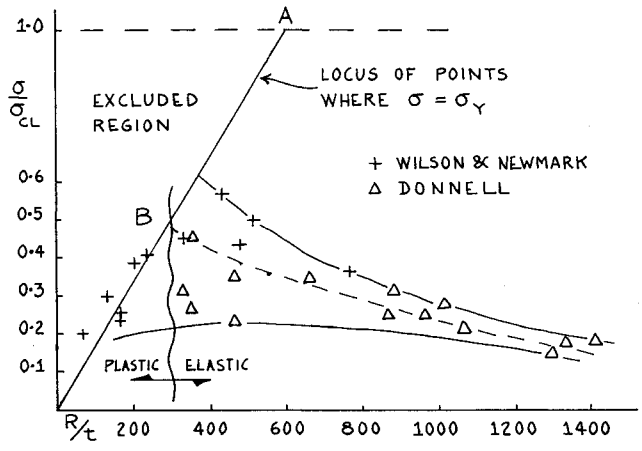

Fig. 2 Distribution of test results on steel cylinders.

The critical R/t is then defined by point B and is approximately equal to 300. This is the value observed from a consideration of the change in behavior of n alone, as shown in Fig. 1.

The division of the behavior of cylinders into elastic and plastic buckling modes has been obscured by the common practice of plotting the results of all cylinder tests on a single σ/σ_{cl} vs R/t plot, regardless of the elastic properties of the cylinder material. A proper consideration of this division greatly reduces the scatter of the data for low values of R/t, where some cylinders fail plastically and others elastically.

Analysis: Elastic Region

If the stress at which buckling occurs is considered, the following effects for elastic buckling appear.

1) For a given L/R, n increases as R/t increases, that is, as σ/σ_{cl} decreases.

2) For a given R/t, n decreases as L/R increases, in which case σ/σ_{cl} either remains constant or, as suggested experimentally,[2, 5] decreases.

In other words, a given value of σ/σ_{cl} is not necessarily associated with a specific n as might be supposed from the plastic buckling analysis. It is difficult to see why elastic buckling should differ from plastic buckling in this respect if the postbuckling load deflection curves are identical for different geometries. It is possible to suppose that the longer shells release more energy upon buckling and thereby break through to a configuration of lower n, and conversely, that the more imperfect shells of higher R/t exhibit less snap through than the better shells of lower R/t, and thus attain equilibrium in a configuration of higher n.

On the other hand, an increase in n occasioned by an increase in R/t and a decrease in σ/σ_{cl} could imply a down-

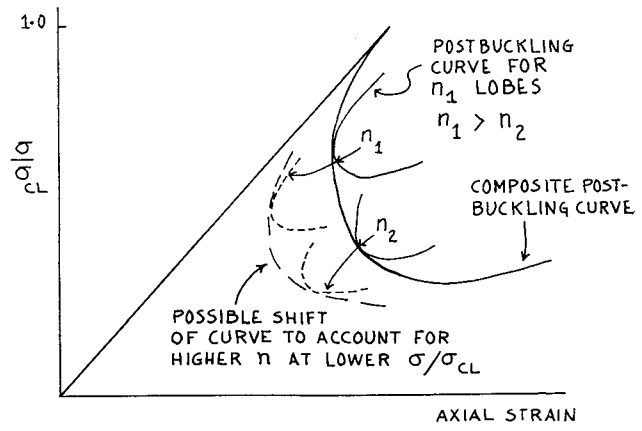

Fig. 3 Postbuckling curves.

Received June 3, 1964; revision received October 5, 1964.
* Graduate Student, Department of Civil Engineering.

ward shift of the postbuckling curves. This is illustrated in Fig. 3. Such a downward shift would explain why σ/σ_{cl} decreases as R/t increases.

Conclusion

The number of circumferential buckling lobes n is a function of L/R and R/t. The nature of this dependency poses a new problem in the understanding of the mechanism of buckling of circular cylinders under axial load. The author is now conducting an extensive series of tests on Mylar cylinders to investigate this mechanism.

References

[1] Wilson, W. N. and Newmark, N. M., "The strength of thin cylindrical shells," Univ. of Illinois Bull. **255** (1933).

[2] Donnell, L. H., "A new theory for the buckling of thin cylinders under axial compression and bending," Trans. Am. Soc. Mech. Engrs. **56**, 795–806 (1934).

[3] Von Karman, T. and Tsien, H.-S., "The buckling of thin cylindrical shells under axial compression," J. Aeronaut. Sci. **8**, 303–312 (1941).

[4] Thielemann, W. F., "On the postbuckling behavior of thin cylindrical shells," NASA TN D-1510, pp. 203–216 (1962).

[5] Ballerstedt, W. and Wagner, H., "Versuche ueber die Festigkeit duenner unversteifter Zylinder unter Schub- und Laengkraeften," Luftfahrtforschung **13**, 309–312 (1936).

Drag on Blunt Bodies with and without Spikes in Low-Density Hypersonic Flow

WILLIAM H. SIMS,* DAVID E. BOYLAN,† AND JERRY S. HAHN‡
ARO Inc., Arnold Air Force Station, Tenn.

Nomenclature

C_∞ = Chapman-Rubesin constant $(\mu_W T_\infty)/(\mu_\infty T_W)$
$C_D{}^*$ = normalized drag coefficient $(C_D - C_{D_i})/(C_{D_{FM}} - C_{D_i})$
L = see Fig. 1
L_{spike} = see Fig. 1
M_∞ = freestream Mach number
$Re_{\infty,D}$ = Reynolds number based on body diameter and freestream conditions
$Re_{\infty,L}$ = Reynolds number based on length L and freestream conditions
T_0 = reservoir temperature of gas
T_W = body wall temperature
$\bar{V}_\infty$ = viscous interaction drag parameter, $M_\infty(C_\infty/Re_{\infty,L})^{1/2}$

THE subject of reducing the drag forces and heating rates by the use of spikes has received much attention in the past.[1–3] Although these studies have encompassed a wide range of Mach number, they have been restricted to conditions of relatively high Reynolds number and do not indicate the viscous interaction effects that planetary entry vehicles encounter at very high altitudes.

For the speed regime of satellite vehicles entering the earth's atmosphere, the necessity of minimizing convective heating led to blunt nose shapes. However, as velocities increase to interplanetary speeds, radiation heating assumes a more important role than does convective heating, reviving interest in the more slender configurations. When the roles of drag coefficient and heat-transfer coefficient are considered in minimizing the ratio of heat transfer to drag coefficients,[4] the desired nose shape then is much more sharp. Because earlier experiments have revealed the effect of low Reynolds number on the drag of a type of blunt body of interest for planetary probes and earth satellites,[5] a program was undertaken to investigate the drag of the same shape after modification to what might be considered a low-drag, low-radiation-heating configuration by addition of a nose spike.[6]

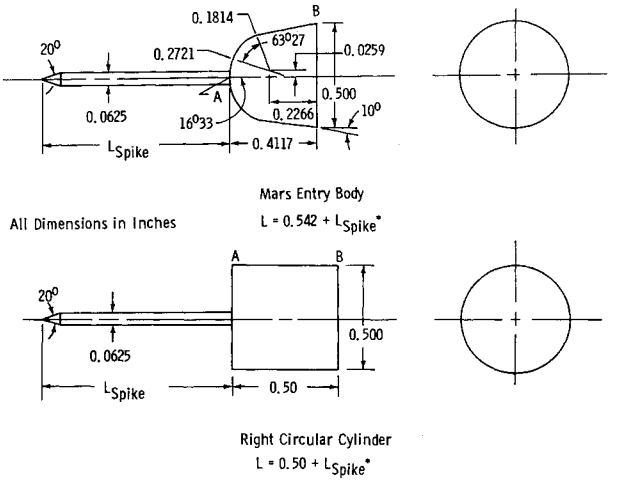

Fig. 1 Model dimensions.

The gas dynamic wind tunnel, Hypersonic (*L*)[7] of the von Kármán Gas Dynamics Facility, at the Arnold Engineering Development Center, was used. This investigation concerned the aerodynamic drag at various angles of attack for a Mach number of 10.1 and a Reynolds number, based on wetted length, of 200 to 1200. The spike lengths tested varied from 0 to 5.0 body diameters.

The configurations of the models may be seen in Fig. 1. The right circular cylinder was only tested at 0° angle of attack. The data have been reduced to coefficient form and are presented as functions of both L_{spike}/D_{base}, and the viscous interaction parameter

$$\bar{V}_\infty = M_\infty(C_\infty/Re_{\infty,L})^{1/2}$$

where

$$C_\infty = (\mu_W T_\infty)/(\mu_\infty T_W)$$

$$Re_{\infty,L} = U_\infty \rho_\infty L/\mu_\infty$$

and L is the characteristic length as described in Fig. 1. The coefficient $(C_\infty)^{1/2}$ was essentially constant ($\approx$0.83) for this investigation.

Figure 2 indicates the influence of the viscous effects as $\bar{V}_\infty$, α, and L_{spike}/D_{base} vary. Here it may be noted that the reduction in $\bar{V}_\infty$ was a result of the model characteristic length L increasing as spike length increased. Thus, one cannot separate the effects of varying $\bar{V}_\infty$ and L_{spike}/D_{base} in Fig. 2. This is done in a later figure.

The variation of C_D with $\bar{V}_\infty$ for various angles of attack also is shown in Fig. 2. Here a very revealing effect occurs which is undoubtedly due to the predominant viscous effects on the spikes. Whereas in earlier studies reductions in C_D were realized for larger Reynolds numbers even at larger angles of attack when spikes were incorporated in the body, this is no longer true for the present tests. For increasing spike length and angle of attack, above approximately 25° in this particular case, the spike causes drag to increase.

Received August 13, 1964. This work was sponsored by Arnold Engineering Development Center, Air Force Systems Command, U. S. Air Force, under Contract No. AF40(600)-1000.

* Engineer, Research Branch, von Kármán Gas Dynamics Facility. Associate Member AIAA.

† Engineer, Research Branch, von Kármán Gas Dynamics Facility.

‡ Co-op Student, University of Cincinnati and von Kármán Gas Dynamics Facility.